

A Prototype Biosensor-Integrated Image-Guided Surgery System

Luke A. Reisner¹, Brady W. King¹, Michael D. Klein², Gregory W. Auner¹,
Abhilash K. Pandya¹

¹ Department of Electrical and Computer Engineering, Wayne State University, Detroit, MI, USA

² Department of Pediatric Surgery, Children's Hospital of Michigan, Detroit, MI, USA

Correspondence to: Abhilash K. Pandya, 5050 Anthony Wayne Dr. #3160, Detroit, MI 48202, USA

E-mail: apandya@ece.eng.wayne.edu

Abstract

Background: In this paper, we investigate the integration of a Raman spectroscopy-based biosensor with an image-guided surgery system. Such a system would provide a surgeon both a diagnosis of tissue being analyzed (e.g. cancer) and localization information displayed within an imaging modality of choice. This type of mutual and registered information could lead to faster diagnoses and enable more accurate tissue resections.

Methods: A test bed consisting of a portable Raman probe attached to a passively articulated mechanical arm was used to scan and classify objects within a phantom skull.

Results: The prototype system was successfully able to track the Raman probe, classify objects within the phantom skull, and display the classifications on medical imaging data within a virtual reality environment.

Conclusion: We discuss the implementation of the integrated system, its accuracy, and improvements to the system that will enhance its usefulness and further the field of sensor-based computer-assisted surgery.

Keywords: Sensor integration, image-guided surgery, Raman spectroscopy, cancer diagnosis, medical robotics

Introduction

Current techniques in image-guided surgery (IGS) rely primarily on visual feedback from the surgical site. In this paper, we address the issue of extending this feedback by adding a sensing modality, Raman spectroscopy, to the already successful techniques of image guidance. It is hypothesized that other modalities of information from the surgical/tumor site based on these non-visual (biochemical) aspects will enhance the surgeon's ability to more completely define resection margins.

The integration of image-guided surgery with advanced sensor technology has been discussed as having great significance for the future of medical procedures. For example, the necessity for diagnostic-based image-guided systems was clearly stated as one of the major goals by a 2002 NIH workshop report on image-guided interventions (1): "There is a critical need to improve sampling techniques for verification of the disease status of an organ system or lesion (for example, to permit correlation of molecular signatures using tissue array analysis with *in vivo* molecular or other imaging/spectroscopy signatures)." We believe that the work discussed in this paper

represents first steps in accomplishing these goals.

Conventional histopathology lacks both the capability for providing immediate feedback and the precision to quantify the extent of disease, particularly in the early stages. Final results usually require 12–24 hours. Even the examination of the more immediate frozen sections requires at least 20 minutes from the time the tissue is removed until the time an answer is available. During tumor-removal surgeries (e.g. for brain cancer), this means the patient must remain open for a longer operative time.

Raman spectroscopy is a technique capable of detecting normal and abnormal regions of tissue (2). Its near-real-time analysis and the fact that it does not require sample preparation make it highly suited for *in vivo* applications (3, 4). Image-guided surgery helps the surgeon position and track instruments (such as a Raman probe) inside the body (5), making it a natural complement for Raman spectroscopy. Integration of this sensing technology with IGS should help maximize its usefulness for *in vivo* applications. Thus, this paper investigates the integration of a Raman probe with an image-guided surgery system for the future diagnosis of cancer.

Raman Spectroscopy

Raman spectroscopy is a near-real-time technique that measures the wavelength and intensity of light inelastically scattered from molecules. In Raman spectroscopy, a specimen is irradiated with a laser light, resulting in the scattering of light due to its interaction with the vibrating molecules in the sample. The majority of scattered light has unchanged frequencies (Rayleigh scattering), whereas the rest is shifted in frequency (Raman scattering) by an amount characteristic of the frequency of the vibrating molecules. These vibrations are a function of molecular conformation, the distribution of electrons in the chemical bonds, and the

molecular environment. Disease leads to changes in the molecular composition and morphologic appearance of affected tissues. Since Raman spectroscopy is sensitive enough to detect these molecular changes, it is a logical choice for the diagnosis of cancer (3, 6–13). This technique is also well-suited for *in vivo* applications because it is non-destructive and requires no sample preparation or contrast-enhancing agents. These features make it appealing for real-time medical diagnosis.

Using recent developments in near-infrared Raman spectroscopy, *in vivo* real-time cancer diagnosis has been attempted during breast surgery (4). Raman spectroscopy offers many opportunities for the development of sensitive diagnostic tools for rapid identification of pathogenic microorganisms (14), assessing tissue specimens including tumor grade types (15, 16), performing continuous patient monitoring (e.g. blood analysis), guiding of surgical interventions, and intraoperative tumor border determination. Since the differentiation of tissue is possible, it is predicted that Raman spectroscopy may soon become a valuable tool to assist in clinical pathology (17).

Our team has been researching the potential of Raman spectroscopy for tumor detection (18–20). In 2005–6, we studied 143 human tissues samples (22 from normal tissues and 121 from tumors) and collected approximately 1700 Raman spectra. This library of Raman data has been analyzed using a variety of statistical techniques, such as principle component analysis and discriminant function analysis, and we are developing learning algorithms based on artificial neural networks and support vector machines to classify the data.

Image-Guided Surgery

During complex operations, surgeons must maintain a precise sense of three-dimensional anatomical relationships (21). In addition, they must use their judgment, experience, and

pathological evaluation (biopsy) to determine resection boundaries. Image-guided surgery fuses medical imaging, computer visualization, and real-time tracking of medical tools to provide the surgeon with a more detailed view of the patient's anatomy. In addition, image-guided surgery has allowed the development of minimally invasive surgical systems, which can greatly reduce cost, surgeon strain, and patient recovery time.

There are two different types of visualization technology that we are researching for the medical domain: augmented reality (AR) and virtual reality (VR) (22-24). Image guidance is an example of VR. Surgeons can now "see" on a 3D image where their tracked surgical tools are with respect to the lesion responsible for the patient's problems. This technology is now starting to be used in several branches of surgery, such as neurosurgery, spinal surgeries (25), orthopedic surgery (26), dental surgery, and even some examples of general surgery (27).

An AR system generates a composite view for the user that includes the live view fused (registered) with either pre-computed data

(e.g. 3D geometry) or other registered sensed data (28). AR is an extension of VR that represents a middle ground between computer graphics in a completely synthetically-generated world (as in VR) and the real world (29-31). Recently, we have developed a system that simultaneously allows the surgeon to have both an AR and VR view of the patient's data (32).

Merging visualization technology with sensor technology will enable surgeons to accurately locate and classify tissues within the body. Hence, we believe the next step is to integrate visualization with sensor technology, specifically a Raman probe. Technology that integrates imaging and sensor information in real-time will add new dimensions to what can be done to diagnose and treat patients (33, 34).

Materials and Methods

The goal of this work is to create a system to detect cancerous tissue in the human body. However, since this paper focuses on the integration and visualization of Raman spectroscopy with image-guided surgery, we can use a phantom model instead of actual tissue. Once the work is more developed, we

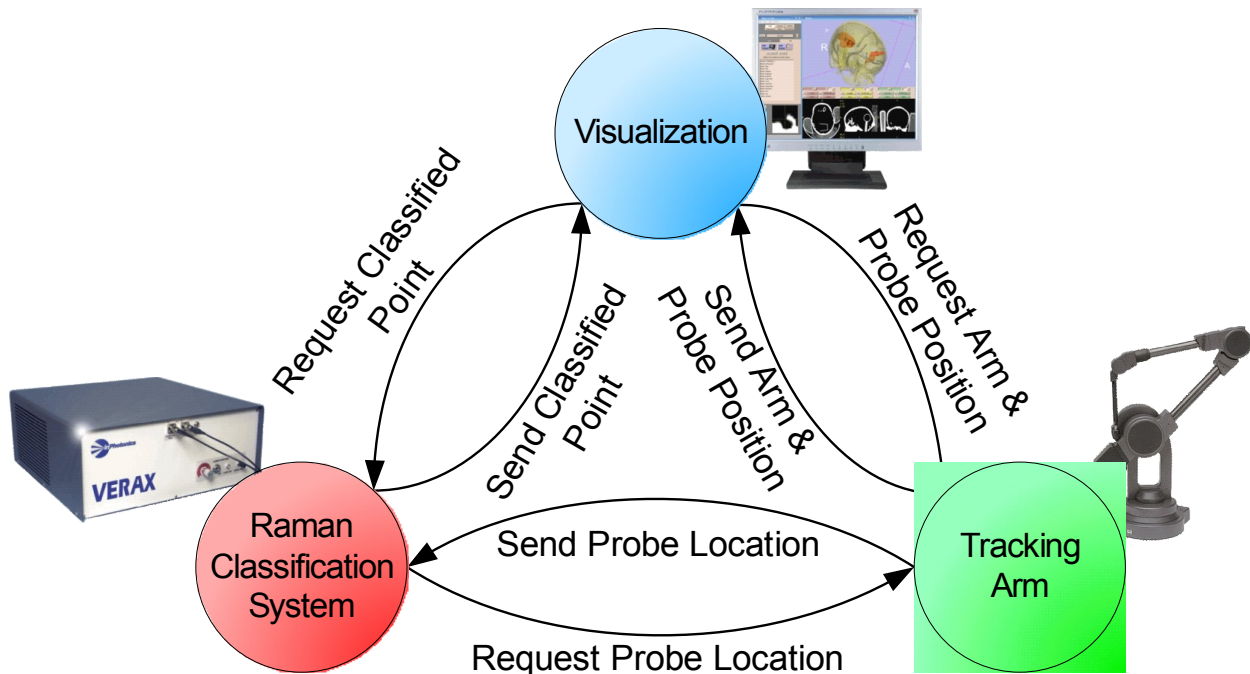


Figure 1: Organization of the system components and the software messages sent among them

can test it on animal and human models. We know from other literature and our own research that Raman spectroscopy is capable of detecting cancerous tissue quickly and accurately (2, 4, 9, 19, 20). Therefore, this work has the potential to extend to real tissue.

Thus, in order to evaluate the integration of Raman spectroscopy and image-guided surgery, we developed a system utilizing several components (see Figure 1). A portable Raman spectrometer was attached to a passively articulated mechanical arm. We also implemented classification algorithms for Raman spectra. The results of the classification are sent to a medical visualization system. Once these systems were integrated together, testing was done with a phantom skull (shown in Figure 2). The skull was filled with various plastic and rubber objects, and CT images were obtained. The entire system was then used to scan objects in the skull, classify the resulting spectral data, and then place markers within our visualization system. Each of the subsystems is described in greater detail below.

Tracking Arm

To track the position of a Raman spectrometer, we attached one to a passively articulated arm, a MicroScribe G2X (Immersion, San Jose, CA), as shown in Figure 2. This arm has five degrees of freedom and, based on our previous research (24), provides joint feedback with an accuracy of 0.87 mm. It was chosen because it is simple to use and its tracking accuracy is within acceptable limits.



Figure 2: The Raman probe, attached to the end of the tracking arm, is used to scan a plastic cup and other objects within the phantom skull

We developed a software application that registers the MicroScribe with patient imaging data and tracks the location of its end-effector. The tracking is accomplished by passing the arm's angular joint feedback through a forward kinematics model of the MicroScribe. The tracking data is relayed in real-time to our visualization system. In the following section, the technical details of our tracking software are presented.

Tracking Algorithms

Our forward kinematics model of the MicroScribe is expressed in Craig's modified Denavit–Hartenberg (DH) notation (35). DH notation provides a compact way to represent the structure of a robot (including link lengths, joint types, and joint angles). The DH

parameters of the MicroScribe are shown in Table 1.

Homogeneous transformation matrices are efficient mathematical structures that can be used to translate between different frames of reference (35). Our tracking system uses these matrices to establish the spatial relationships among the MicroScribe arm, Raman probe, patient (phantom skull), and patient imaging (CT scan data). This enables us to track the location of the MicroScribe with respect to the phantom skull and overlay this information on the CT scan data in our visualization system.

In order to track the MicroScribe's end-effector relative to the skull, we execute a pair-point-matching algorithm between seven common fiducials on the phantom skull and its CT scan data. The algorithm uses an iterative Levenberg–Marquardt optimization method to establish a homogeneous transformation from the skull (S) to the base of the MicroScribe (B), $T_{S,B}$.

The next step in tracking the MicroScribe is to determine the location of its end-effector (EE) relative to its base. This is done by multiplying a series of transformation matrices that represent the position and orientation of each of the MicroScribe's joints (J_i) relative to the previous joint (J_{i-1}):

$$T_{B,EE} = T_{B,J1} \cdot T_{J1,J2} \cdot T_{J2,J3} \cdot T_{J3,J4} \cdot T_{J4,J5} \cdot T_{J5,EE}$$

Equation 1

Each transformation matrix is generated via the following formula, which uses the joint angles (θ_i) and other DH parameters given in the rows of Table 1:

$$T_{J_{i-1},J_i} = \begin{bmatrix} \cos \theta_i & -\sin \theta_i & 0 & a_{i-1} \\ \sin \theta_i \cos \alpha_{i-1} & \cos \theta_i \cos \alpha_{i-1} & -\sin \alpha_{i-1} & -d_i \sin \alpha_{i-1} \\ \sin \theta_i \sin \alpha_{i-1} & \cos \theta_i \sin \alpha_{i-1} & \cos \alpha_{i-1} & d_i \cos \alpha_{i-1} \\ 0 & 0 & 0 & 1 \end{bmatrix}$$

Equation 2

Finally, we can combine the transformation from the skull to the base with the transformation from the base to the end-

effector to produce the desired transformation from the skull to the end-effector:

$$T_{S,EE} = T_{S,B} \cdot T_{B,EE}$$

Equation 3

This transformation from the phantom skull to the end-effector allows our visualization system to display the location of the MicroScribe's tip relative to the 3D CT imaging of the skull.

To track the Raman probe, which is attached to the MicroScribe, the kinematic model for the MicroScribe was extended by adding an extra transformation from the end-effector to the tip of the Raman probe (RP):

$$T_{EE,RP} = \begin{bmatrix} 1 & 0 & 0 & -14.2875 \\ 0 & 1 & 0 & 0 \\ 0 & 0 & 1 & -268.2875 \\ 0 & 0 & 0 & 1 \end{bmatrix}$$

Equation 4

Combining Equation 3 and Equation 4 allows the computation of the transformation from the skull to the tip of Raman probe:

$$T_{S,RP} = T_{S,EE} \cdot T_{EE,RP}$$

Equation 5

This transformation allows the probe to be tracked in our visualization system relative to the skull's CT scan data.

Table 1: Denavit–Hartenberg parameters for the MicroScribe G2X mechanical arm. The non-zero (θ_i) terms represent variable joint angles.

i	a_{i-1} (mm)	d_i (mm)	α_{i-1} (rad)	θ_i (rad)
1	0	210.82	0	(θ_1)
2	24.18	-22.53	0.4999π	(θ_2)
3	260.68	-0.30	-0.0002π	(θ_3)
4	13.89	234.70	0.4972π	(θ_4)
5	-10.26	8.10	-0.5007π	(θ_5)
6	10.16	-134.16	-0.4994π	0

Raman Spectrometer

The portable Raman spectrometer we use is a Verax (InPhotonics, Norwood, MA). It is shown in Figure 3. This device uses a fiber optic probe and a 785 nm, 300 mW laser beam to obtain Raman spectra with an accuracy up to 4 cm^{-1} . The end of the probe is a long tube, 1 cm in diameter, thus making it suitable for a test bed for minimally invasive surgery. In addition, the probe can be sterilized via an autoclave.

The Raman probe (shown in Figure 2) was affixed to the MicroScribe using a simple clamping system. The end-effector of the MicroScribe was marked to ensure consistent placement, allowing the probe to be detached and reattached.



Figure 3: The Verax portable Raman spectrometer with an attached fiber optic probe

Raman Classification

Many techniques have been developed for the classification of Raman spectra. For our implementation, we used a method based on artificial neural networks, which have been shown to perform well for Raman classification (36-38).

A variety of preprocessing tasks are performed on the raw Raman spectral data, including background fluorescence subtraction (via adaptive polynomial fitting), median noise filtering, normalization, and peak extraction. Due to the high dimensionality of Raman spectra, we used principle component analysis

to select the most significant spectral peaks for algorithm consideration.

Our neural network is a two-layer feedforward perceptron network. There is one input for each spectral peak extracted during the preprocessing phase and one output for each possible class (e.g. plastic vs. rubber or healthy vs. cancerous tissue). The hidden layer uses hyperbolic tangent activation functions, and the output layer has logistic sigmoid activation functions. For this application, the network used 10 hidden neurons and was trained via backpropagation. The final output was the classification of the scanned tissue/material and a percentage indicating the confidence of the neural network.

Visualization

The visualization for our image-guided surgery system is implemented using 3D Slicer (www.slicer.org), an open-source application for displaying medical data. 3D Slicer provides a virtual reality environment in which various imaging modalities (e.g. CT or MRI data) can be presented. The software includes the ability to display the locations of objects with respect to 3D models that are derived from segmentation of the medical imaging.

We modified 3D Slicer in several ways to adapt it to our application. First, we developed a TCP/IP interface that receives the tracking data for the MicroScribe and displays its position in the VR environment relative to the

medical imaging data. This allows us to track the Raman probe in real-time. Second, we developed a way to place colored markers that indicate tissue/material classification on the medical imaging data. The combination of these modifications enables us to denote the location and classification of tissue/material scanned with the probe in near-real-time.

Results

As described in the Materials and Methods section, we used the completed system to scan objects within a phantom skull. The MicroScribe and probe were positioned manually and tracked in real-time during this test. The collected Raman spectra were

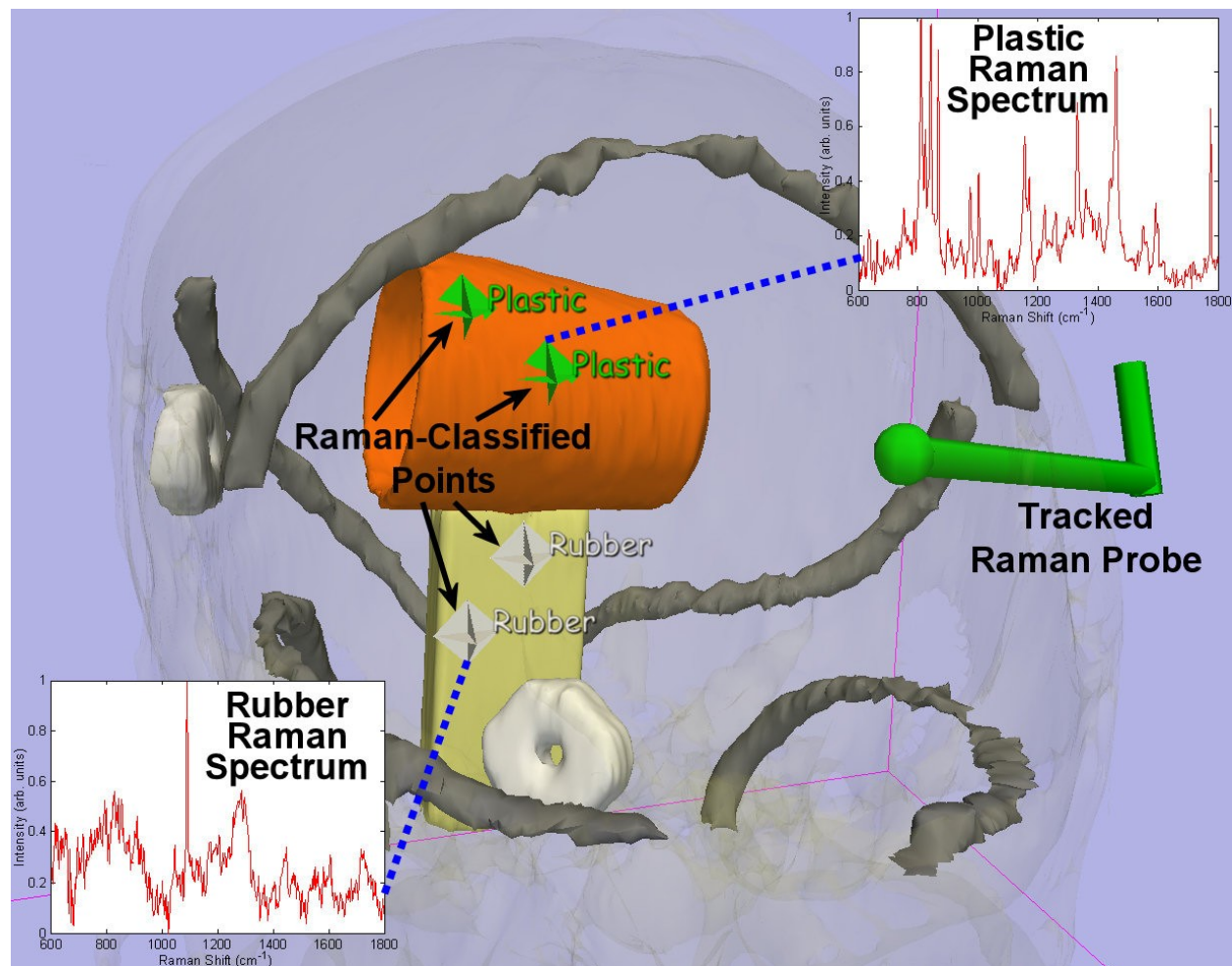


Figure 4: A screenshot of our visualization system showing 3D models (derived from CT imaging of the phantom skull), the location of the tracked Raman probe, collected Raman spectra, and colored markers denoting the classifications (computed from Raman scan data) of various objects within the skull

classified and displayed as colored markers in our visualization system. This is shown in Figure 4.

The system performed as expected. The tracking of the probe, the classification of the Raman spectra, and the display of the colored markers all occurred in real-time. The only major delay was caused by the scanning of the tissue by the Raman probe, which requires roughly 5 seconds to produce a scan with a reasonable signal-to-noise ratio.

The Raman scans were able to distinguish between the plastic and the rubber objects. The corresponding markers in the visualization display correctly reflected the classifications that were made. The positions of the markers were also accurate with respect to the locations from which scans were taken. Since the setup of the system is very similar to that of our previous work (24), we estimate that the probe tracking accuracy is around 1 mm.

Discussion

In a paper discussing the future of computer-assisted and robotic surgery (39), Taylor and Stoianovici stated that it will become increasingly important to design systems that can incorporate a wide range of biomedical sensors and that can work with multiple imaging modalities. We provide an example of this goal with the successful integration of Raman spectroscopy with an image-guided surgery system, demonstrated using a phantom skull. Our system, which tracks an image-registered Raman probe, is developed in a manner that allows the results of neural network-classified Raman data to be displayed directly on any imaging modality of the phantom's anatomy, all in near real-time.

This paper demonstrates that Raman spectroscopy and image-guided surgery can be combined to provide a powerful diagnostic system. Even though we have used a phantom model, the underlying technologies have been previously shown to work with human tissue. With further research, we believe this system

will be suitable for human applications. For now, we will continue to develop and test the system using phantom models. In the future, we plan to evaluate the system with animal testing. Eventually, we hope to apply our work to human cases. If the results continue to be positive, we believe that Raman spectroscopy has the potential to be a powerful complement to conventional histopathology.

To our knowledge, there have been no other prototypes in the literature that attempt to combine Raman spectroscopy and image-guided surgery. We conjecture that a system based on these technologies could eventually provide many benefits in the surgical environment. These benefits could include faster diagnoses and more accurate resections, hence producing better patient outcomes. However, there are certain issues that need detailed research and development.

One key issue is the size of the Raman probe. Ideally, the entire instrument should be about the size of a scalpel for easy manipulation by the surgeon. Existing portable systems are still too bulky as real-time diagnostic tools for certain applications. The availability of miniaturized hand-held devices would create a platform for a wider range of research on real-time tissue diagnostics. Once developed, this technology will enable the creation of a whole new field of real-time, *in vivo* spectroscopic diagnostics of tissue.

Another relevant issue is the positional accuracy of the image-guided Raman system. Although the tip of our Raman probe can be tracked to within an acceptable accuracy for neurosurgery, there is an uncertainty of about 5 mm (the diameter of the probe's transmission window) as to exactly where the human-held probe actually measures the point of interest. A system in which the actual point of interest could be better determined and more accurately placed would be much more useful. The issues of placement accuracy and the requirement of holding the sensor still during acquisition can be alleviated by the

closely related field of medical robotics. A robot can accurately place and steadily hold a probe in the surgical environment.

Thus, we plan to expand the work described in this paper to include the Aesop 3000 medical robot (Intuitive Surgical, Sunnyvale, CA). This robot will be used to actively position the Raman probe instead of the passive MicroScribe arm. This will provide several benefits over the current system. First, the Aesop will be able to hold the probe completely steady during a scan, which is important considering scans can take 5 or more seconds. Second, the Aesop will be able to position the probe more accurately using medical imaging data, enabling the surgeon to precisely scan the tissue of interest. Third, automated scanning will be possible, in which the Aesop moves among numerous points over a defined area of tissue, taking a Raman scan at each.

Our work with the Aesop 3000 will include a detailed human (surgeon) factors study. Tests will be performed to ensure that the system is beneficial to surgeons. For example, we will verify that the speed and accuracy of tissue diagnoses are improved through the use of the system, and several visualization techniques will be implemented and compared to find the best one. We believe that such testing is necessary during research and development to ensure that the results are a useful addition to the field.

Acknowledgements

This work was supported in part by the Endowment for Surgical Research (ENSURE) at the Children's Research Center of Michigan. The authors would also like to thank Alex Cao and Rachel Weber for their help with Raman spectra processing and Dr. Gulay Serhatkulu for her assistance in collecting Raman spectra.

References

1. NIH/NSF. Final Report. In: Haller JW, Clarke L, Hamilton B, editors. Workshop on Image-Guided Interventions; 2002 September 12-13; Bethesda, MD; 2002.
2. Mahadevan-Jansen A, Richards-Kortum R. Raman Spectroscopy For Cancer Detection: A Review. In: 19th International Conference of IEEE/EMBS; 1997 Oct. 30-Nov. 2; Chicago, IL; 1997. p. 2722-2728.
3. Molckovsky A, Song LM, Shim MG, Marcon NE, Wilson BC. Diagnostic potential of near-infrared Raman spectroscopy in the colon: differentiating adenomatous from hyperplastic polyps. *Gastrointestinal Endoscopy* 2003;57(3):396-402.
4. Haka AS, Volynskaya Z, Gardecki JA, Nazemi J, Lyons J, Hicks D, et al. In vivo Margin Assessment during Partial Mastectomy Breast Surgery Using Raman Spectroscopy. *Cancer Research* 2006;66(6):3317-22.
5. Sauer F. Image Registration: Enabling Technology for Image Guided Surgery and Therapy. In: 27th Annual International Conference of the IEEE Engineering in Medicine and Biology Society; 2005 September 1-4; Shanghai, China; 2005. p. 7242-7245.
6. Crow P, Stone N, Kendall CA, Uff JS, Farmer JA, Barr H, et al. The use of Raman spectroscopy to identify and grade prostatic adenocarcinoma in vitro. *Br J Cancer* 2003;89(1):106-8.
7. Krafft C, Miljanic S, Sobottka SB, Schackert G, Salzer R. Near-infrared Raman spectroscopy to study the composition of human brain tissue and tumors. *Proceedings of SPIE-The International Society for Optical Engineering* 2003;5141(Diagnostic Optical Spectroscopy in Biomedicine II):230-236.

8. Frank CJ, Redd DC, Gansler TS, McCreery RL. Characterization of human breast biopsy specimens with near-IR Raman spectroscopy. *Anal Chem* 1994;66(3):319-26.
9. Stone N, Kendall C, Shepherd N, Crow P, Barr H. Near-infrared Raman spectroscopy for the classification of epithelial pre-cancers and cancers. *Journal of Raman Spectroscopy* 2002;33(7):564-573.
10. Mahadevan-Jansen A, Mitchell MF, Ramanujam N, Utzinger U, Richards-Kortum R. Development of a fiber optic probe to measure NIR Raman spectra of cervical tissue in vivo. *Photochem Photobiol* 1998;68(3):427-31.
11. Gniadecka M, Wulf HC, Nielsen OF, Christensen DH, Hercogova J. Distinctive molecular abnormalities in benign and malignant skin lesions: studies by Raman spectroscopy. *Photochem Photobiol* 1997;66(4):418-23.
12. Johansson CK, Christensen DH, Nielsen OF. Near-infrared Fourier transform Raman spectral studies of human skin. *Dansk Kemi* 1999;80(8):12-13.
13. Min Y-K, Yamamoto T, Kohda E, Ito T, Hamaguchi H-o. 1064 nm near-infrared multichannel Raman spectroscopy of fresh human lung tissues. *Journal of Raman Spectroscopy* 2005(36):73-76.
14. Maquelin K, Choo-Smith LP, van Vreeswijk T, Endtz HP, Smith B, Bennett R, et al. Raman spectroscopic method for identification of clinically relevant microorganisms growing on solid culture medium. *Anal Chem* 2000;72(1):12-9.
15. Kalasinsky KS, Kalasinsky VF. Infrared and Raman microspectroscopy of foreign materials in tissue specimens. *Spectrochimica Acta A: Mol Biomol Spectroscopy* 2005;61(7):1707-13.
16. Schaeberle MD, Kalasinsky VF, Luke JL, Lewis EN, Levin IW, Treado PJ. Raman chemical imaging: histopathology of inclusions in human breast tissue. *Anal Chem* 1996;68(11):1829-33.
17. Pappas D, Smith BW, Winefordner JD. Raman spectroscopy in bioanalysis. *Talanta* 2000;51(1):131-144.
18. Pandya A, Auner G. Robotic Technology: a Journey into the Future. In: Menon M, Das S, editors. *Robotic Urologic Surgery*: Elsevier, Inc.; 2004. p. 793-800.
19. Thakur JS, Dai H, Shukla N, Serhatkulu GK, Cao A, Pandya A, et al. Raman spectral signatures of mouse mammary tissue and associated lymph nodes: normal, tumor, and mastitis. *Journal of Raman Spectroscopy* 2006;(In press).
20. Lorincz A, Haddad D, Naik R, Naik V, Fung A, Cao A, et al. Raman spectroscopy for neoplastic tissue differentiation: a pilot study. *Journal of Pediatric Surgery* 2004;39(6):953-956.
21. Bucholz RD, Smith KR, Laycock KA, McDurmott LL. Three-dimensional localization: From image-guided surgery to information-guided therapy. *Methods* 2001;25(2):186-200.
22. Gong J, Zamorano L, Li Q, Pandya AK, Diaz F. Development of Universal Instrumentation for Advanced Neuronavigation System. In: *Congress of Neurological Surgeons*; 2001 Sept. 29 - Oct. 4; San Diego, CA; 2001.
23. Pandya A, Siadat M, Speaker) GAI. Augmented Reality vs. Neuronavigation: a Comparison of Surgeon Performance. In: *Biomedical Engineering Symposium* 2003; 2003; Wayne State University; 2003.
24. Pandya A, Siadat MR, Auner G. Design, implementation and accuracy of a prototype for medical augmented reality. *Computer Aided Surgery* 2005;10(1):23-35.
25. Holly LT, Foley KT. Intraoperative spinal navigation. *Spine* 2003;28(15):S54-S61.
26. DiGioia AM. Computer assisted orthopaedic surgery: Medical robotics and

- image guided surgery - Comment. *Clinical Orthopaedics and Related Research* 1998(354):2-4.
27. Cash DM, Sinha TK, Chapman WC, Terawaki H, Dawant BM, Galloway RL, et al. Incorporation of a laser range scanner into image-guided liver surgery: Surface acquisition, registration, and tracking. *Medical Physics* 2003;30(7):1671-1682.
 28. Pandya A, Zamorano L, inventors; Wayne State University, assignee. Augmented Tracking Using Video, Computer Data and/or Sensing Technologies. USA patent application 20030179308. 2002.
 29. Pandya AK, Siadat M, Ye Z, Prasad M, Auner G, Zamorano L, et al. Medical Robot Vision Augmentation—A Prototype. In: *Medicine Meets Virtual Reality*; 2003; Newport Beach, California: Aligned Management Associates, Inc; 2003. p. 85.
 30. Pandya AK, Siadat M, Zamorano L, Gong J, Li Q, Maida JC, et al. Augmented Robotics for Neurosurgery. In: *American Association of Neurological Surgeons*; 2001 April 21-26; Toronto, Ontario; 2001.
 31. Pandya AK, Zamorano L, Siadat M, Li Q, Gong J, Maida JC. Augmented Robotics for Medical and Space Applications. In: *Human Systems*; 2001 June 19; NASA Johnson Space Center, Houston, TX; 2001.
 32. Pandya A, Auner G. Simultaneous Augmented and Virtual Reality for Surgical Navigation. In: *North American Fuzzy Information Processing Society Annual Conference*; 2005 June 22-25; Ann Arbor, Michigan; 2005. p. 429-435.
 33. Samset E, Hirschberg H. Image-guided stereotaxy in the interventional MRI. *Minimally Invasive Neurosurgery* 2003;46(1):5-10.
 34. Nakao N, Nakai K, Itakura T. Updating of neuronavigation based on images intraoperatively acquired with a mobile computerized tomographic scanner: Technical note. *Minimally Invasive Neurosurgery* 2003;46(2):117-120.
 35. Craig JJ. *Introduction to Robotics: Mechanics and Control*. 2nd ed: Addison-Wesley Longman Publishing Co., Inc. Boston, MA, USA; 1989.
 36. Gniadecka M, Philipsen PA, Sigurdsson S, Wessel S, Nielsen OF, Christensen DH, et al. Melanoma Diagnosis by Raman Spectroscopy and Neural Networks: Structure Alterations in Proteins and Lipids in Intact Cancer Tissue. *Journal of Investigative Dermatology* 2004;122:443-449.
 37. de Paula Jr AR, Sathaiah S. Raman spectroscopy for diagnosis of atherosclerosis: a rapid analysis using neural networks. *Med Eng Phys* 2005;27(3):237-44.
 38. Sigurdsson S, Philipsen PA, Hansen LK, Larsen J, Gniadecka M, Wulf HC. Detection of skin cancer by classification of Raman spectra. *IEEE Transactions on Biomedical Engineering* 2004;51(10):1784-1793.
 39. Taylor RH, Stoianovici D. *Medical Robotics in Computer-Integrated Surgery*. *IEEE Trans on Robotics and Automation* 2003;19(5):765-782.